ARTICLE

Influence of Functional Groups and Modification Sites of Metal-Organic Frameworks on CO_2/CH_4 Separation: A Monte Carlo Simulation Study

Jie Gong, Wei Li, Song Li*

State Key Laboratory of Coal Combustion, School of Energy and Power Engineering, Huazhong University of Science and Technology, Wuhan 430074, China
Shenzhen Research Institute of Huazhong University of Science and Technology, Shenzhen 518057, China
Nano Interface Centre for Energy, School of Energy and Power Engineering, Huazhong University of Science and Technology, Wuhan 430074, China

(Dated: Received on May 26, 2017; Accepted on July 5, 2017)

In order to explore the influence of modification sites of functional groups on landfill gas (CO_2/CH_4) separation performance of metal-organic frameworks (MOFs), six types of organic linkers and three types of functional groups (*i.e.* -F, -NH_2, -CH_3) were used to construct 36 MOFs of pcu topology based on copper paddlewheel. Grand canonical Monte Carlo simulations were performed in this work to evaluate the separation performance of MOFs at low (vacuum swing adsorption) and high (pressure swing adsorption) pressures, respectively. Simulation results demonstrated that CO_2 working capacity of the unfunctionalized MOFs generally exhibits pore-size dependence at 1 bar, which increases with the decrease in pore sizes. It was also found that -NH_2 functionalized MOFs exhibit the highest CO_2 uptake due to the enhanced Coulombic interactions between the polar -NH_2 groups and the quadrupole moment of CO_2 molecules, which is followed by -CH_3 and -F functionalized ones. Moreover, positioning the functional groups -NH_2 and -CH_3 at sites far from the metal node (site b) exhibits more significant enhancement on CO_2/CH_4 separation performance compared to that adjacent to the metal node (site a).

Key words: Metal-organic frameworks, Pore-size dependence, Functional groups, Modification sites, Interaction energy

I. INTRODUCTION

The increasing greenhouse gas emission and global warming are drawing worldwide attention. One way to mitigate this trend is switching to CH_4-based energy sources that emit comparatively less CO_2 per unit of energy than coal- or petroleum-based fuels due to their higher hydrogen to carbon (H/C) ratio. Municipal or industrial landfill gas is a promising and potential source to obtain CH_4 [1], however the separation of CO_2 from landfill gas is essential because the presence of a large amount of CO_2 impurities (40% to 60%) greatly reduces the combustion efficiency and is corrosive to pipelines or cylinders [2]. Conventional technologies for CO_2/CH_4 separation include absorption, cryogenic distillation, membrane separation, and adsorption [3]. Among these, vacuum/pressure swing adsorption (VSA/PSA) is promising because of the easy control, low operation cost, and superior energy efficiency [4]. A key issue of designing a VSA/PSA system is selecting a highly selective adsorbent.

Metal-organic frameworks (MOFs), a new class of porous crystalline materials composed of self-assembled metallic species and organic linkers, have widespread applications, included but not limited to gas storage, gas separation, catalysis, thermal conversion, drug delivery, harmful substance storage, and biomedical imaging [5−7]. MOFs exhibit ultrahigh surface areas, controllable pore sizes, and shapes as well as "tailor-made" framework functionalities, hence giving rise to millions of diverse structures due to the various combinations of building blocks and substituents [8, 9]. As promising adsorbents, MOFs have received extensive attention to promote their selectivity and adsorption capacity for CO_2/CH_4 separation [10, 11]. Wilmer *et al.* [12] implemented a large-scale computational screening over 1.3×10^5 hypothetical MOFs, and discovered correlations between structural characteristics (*e.g.*, pore size, surface area, and pore volume), as well as chemical characteristics (*i.e.*, functional groups), for CO_2/CH_4 separation performance. Bae *et al.* [13] studied the adsorption of CO_2 and CH_4 in a mixed-ligand metal-organic framework $Zn_2(NDC)_2$ (DPNI) (NDC=2,6-naphthalenedicarboxylate, DPNI=*N*,*N*′-di-(4-pyridyl)-1,4,5,8-naphthalene tetracarboxydiimide) using volu-

*Author to whom correspondence should be addressed. E-mail: songli@hust.edu.cn

metric adsorption measurements and grand canonical Monte Carlo (GCMC) simulations, in which a selectivity of 30 for CO_2 over CH_4 was reported.

Functionalization has also been shown to impose profound influences on the adsorption properties of MOFs. In 2002, Yaghi's group [14] functionalized MOF-5 with the organic groups -Br, -NH_2, -OC_3H_7, -OC_5H_{11}, -C_2H_4, and -C_4H_4, and the pore size of frameworks can be expanded by the long molecular struts biphenyl, tetrahydropyrene, pyrene, and terphenyl. Deng *et al.* [15] successfully deployed multivariate (MTV) link synthetic strategy to synthesize 18 analogues (also named MTV-MOFs) of MOF-5 with up to eight distinct functionalities in one phase. It was found that the performance of MTV-MOFs is not a simple linear combination of their constituents, and one member of the 18 derivatives exhibits significantly enhanced selectivity towards CO_2 over CO compared to its best same-link counterparts. McDaniel *et al.* [16] reported that the absolute gas uptake normally is not merely a sum of linear contributions from its constituent functionalities but rather exhibits a synergistic enhancement due to cooperative adsorbate-linker interactions involving multiple functionalities. Efforts have also been made to introduce polar functional groups with high affinity towards CO_2 to boost the CO_2/CH_4 separation [17, 18]. Yang *et al.* [19] explored the effects of seven functional groups on the CO_2/CH_4 separation performance of UiO-66(Zr) computationally and found that -SO_3H and -CO_2H functionalized MOFs showed the highest CO_2/CH_4 selectivity, good working capacity, and medium ranged CO_2 adsorption enthalpy. Walton *et al.* [20] synthesized a new monomethyl-functionalized UiO-66 (UiO-66-MM), which exhibited a much higher CO_2/CH_4 selectivity due to the enhanced van der Waals interactions with CO_2. Couck *et al.* [21] reported functionalized MIL-53(Al) with amino groups, whose CO_2/CH_4 selectivity was increased by several orders of magnitude without compensating its CO_2 adsorption capacity. Mu *et al.* [22] found that the counterbalance between the enhanced adsorption resulted from the electron-donating functional groups and the steric hindrance effects of functionality was essential in designing high-performing MOF materials for CO_2/CH_4 separation. Gomez-Gualdron *et al.* [23] found that triple bonds adjacent to the inorganic zirconium nodes provided more efficient methane packing around the nodes at high pressures. Such findings have led us to ponder over the steric effects of modification sites of functional groups. Nonetheless, to the best of our knowledge, little work has been implemented to explore the influence of modification sites or a combination of both modification sites and the type of functional group on CO_2/CH_4 separation.

In order to identify the correlation between the functional groups and their modification sites of MOFs for CO_2/CH_4 separation, 36 MOFs of the same topology assembled from one of the six types of linkers (*i.e.* L1, L2, L3, L4, L5, L6) (FIG. 1) with or without functional groups positioning at varying sites to metal were investigated by grand canonical Monte Carlo (GCMC) simulations. This study may provide molecular insight into effective design of promising MOFs for the CO_2/CH_4 separation.

II. METHODS

A. Construction of hypothetical MOFs

As shown in FIG. 1, the six types of linkers are terephthalic acid (L1), 3,3′-(1,4-phenylene)dipropiolic acid (L2), biphenyl-4,4-dicarboxylic acid (L3), 4,4-stilbenedicarboxylic acid (L4), pyrene-2,7-dicarboxylic acid (L5), and 4,4′-ethyne-1,2-diyldibenzoic acid (L6), respectively. MOFs comprised of these linkers are named as MOF 1−6 accordingly, and each MOF consists of only one type of linkers. Three types of functional groups, -F, -NH_2, and -CH_3 were chosen as representatives of functionalities with different affinities towards CO_2 adsorbates, and positioned to symmetrical sites of aromatic ring as highlighted in FIG. 1. According to FIG. 1, L1 and L2 only have one type of modification sites, while L3−L6 possess two types of modification sites: adjacent to the metal node (denoted as site a) and far from the metal node (denoted as site b). According to the definitions above, the MOF derivatives are named by integration of the linker type, modification sites, and functional group, *e.g.* MOF 1-CH_3 and 5b-NH_2. Density functional theory (DFT) structure optimization of all MOF derivatives was conducted to ensure that they are geometrically and chemically meaningful, and it is observed that introducing functional groups does not induce significant structural change.

B. Computational details

Grand canonical Monte Carlo (GCMC) simulations were conducted to obtain CO_2 adsorption performance of MOFs. Transferable potentials for phase equilibria (TraPPE) force field parameters [24] were used for CO_2 and CH_4 adsorbates, and Lorentz-Berthelot mixing rules were used to calculate the van der Waals interaction parameters between the atoms of MOFs and adsorbates. Universal force field (UFF) [25] and density-derived electrostatic and chemical (DDEC) [26] partial charges were employed for atoms of both framework and functional groups. The reliability of UFF force field has been validated in previous works [27, 28]. DDEC partial charges were calculated by fitting the electrostatic potential surface from the plane-wave density functional theory (DFT) calculations using the Vienna *ab initio* software package (VASP) [29−31]. The electron-ion interaction was described by the projector augmented wave (PAW) scheme with an energy cutoff of 450 eV. A 1×1×1 Monkhorst-Pack k-point mesh in the reciprocal

DOI:10.1063/1674-0068/31/cjcp1705108

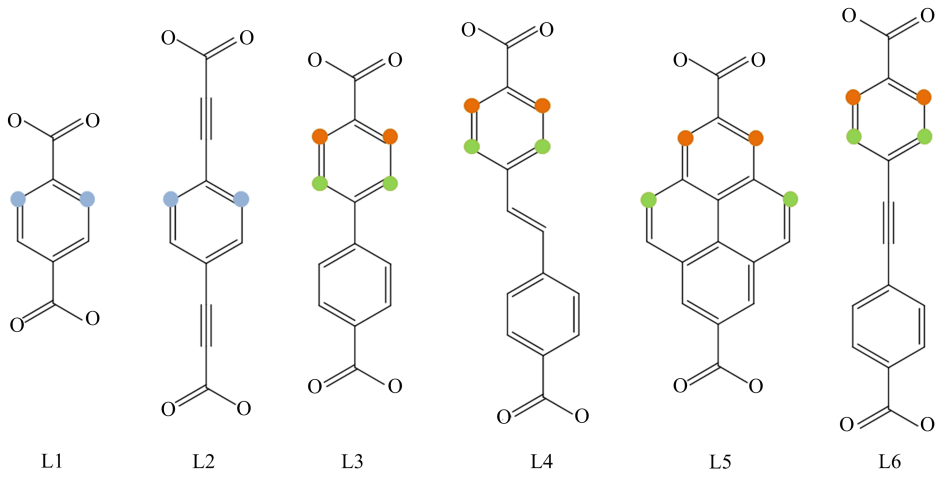

FIG. 1 Illustration of six types of linkers and two modification sites: L1, L2, L3, L4, L5, L6. The sites in orange and green refer to modification sites that are close to site a and far from site b the metal node respectively, and sites in light blue mean that there is only one type of modification sites on the linker.

space with spin polarization was adopted for Brillouin zone sampling.

GCMC simulations were conducted in version 1.9 of RASPA simulation code [32]. The functionalized and geometrically modified MOF derivatives were used for GCMC simulations and all atoms of MOFs were held fixed during the simulations. Ewald method was employed for describing the long-range electrostatic interactions [33]. All the interatomic interactions were modeled using the standard 12-6 Lennard-Jones (LJ) potential and Coulombic potential, both of which adopt a cutoff of 12.8 Å. Each simulation cell was replicated in all three dimensions to ensure the cell length was more than twice of the cutoff. All simulations consist of an equilibration of 5×10^4 Monte Carlo cycles followed by another 5×10^4 cycles to obtain the ensemble-averaged properties. Each cycle contains N Monte Carlo moves including insertion, deletion, translation, rotation, and identity change of adsorbates with equal probabilities, where N equals to the number of molecules in the simulation at the beginning. Monte Carlo moves including translation, rotation, reinsertion, and deletion of adsorbate molecules were performed with equal probabilities. All calculations were conducted at 298 K.

The adsorption working capacity was computed by subtracting the CO_2 adsorption capacity of a MOF at 0.1 bar from that at 1 bar under the vacuum-swing adsorption (VSA) conditions and subtracting the CO_2 adsorption capacity at 1 bar from that at 5 bar under the pressure-swing adsorption (PSA) conditions [34]. The CO_2/CH_4 selectivity of CO_2/CH_4 gas mixture with a molar ratio of 1:1 at 1 and 5 bar was calculated using the following equation, respectively.

$$S_{CO_2/CH_4} = \frac{q_{CO_2}/p_{CO_2}}{q_{CH_4}/p_{CH_4}} \quad (1)$$

where q refers to the gas uptake of MOFs from gas mixture and p is the partial pressure of the adsorbates. Helium void fraction and surface area (SA) were computed in RASPA as well. Largest cavity diameter (LCD) and pore limiting diameter (PLD) were obtained from the Zeo++ package [35].

III. RESULTS AND DISCUSSION

The helium void fraction (HVF), surface area (SA), largest cavity diameter (LCD), and pore limiting diameter (PLD) of functionalized and unfunctionalized MOFs are provided in Table I. It is found that the LCDs of parent structures follow the order of MOF 1<5<3<2<4<6, and functionalization does not bring about significant change in the SA or pore size of frameworks. Besides, functionalization at site b generally results in slightly smaller LCD, and slightly larger SA compared to site a.

The calculated CO_2 working capacity and CO_2/CH_4 selectivity of all MOF derivatives at VSA conditions are shown in FIG. 2. It was observed that CO_2 uptake of the six parent MOFs decreases in the order of MOF 1>5>3>2≈4>6, which is in exactly opposite trend to their variations in LCDs: MOF-1<5<3<2<4<6, suggesting the high CO_2 adsorption in small pores, consistent with previous report [36]. The density distribution map in FIG. 3 also evidenced the highest CO_2 adsorption in MOF-1, and the adsorbed CO_2 molecules were mostly adjacent to the metal node. Regarding the functionalization effects, the CO_2 working capacity of the functionalized MOFs exhibits the order of -NH_2>-CH_3>parent>-F except for 4a, where 4a-CH_3 and 4a-NH_2 exhibit similar working capacity. It was also illustrated that the CO_2/CH_4 selectivity of the vast majority of MOFs presents similar tendency to CO_2 working capacity except for 3a-F and 4a-F, whose selectivities are slightly higher than their parent counterparts. The

DOI:10.1063/1674-0068/31/cjcp1705108

TABLE I Results of helium void fraction (HVF), surface area (SA), largest cavity diameter (LCD), and pore limiting diameter (PLD). LCD and PLD were calculated from the Zeo++ package [35]. Helium void fraction and SA were calculated using helium and nitrogen as the probing atom, respectively at 298 K and 1 bar in RASPA.

Name	HVF	SA/(m^2/g)	LCD/Å	PLD/Å
1	0.70	2495.57	9.32	7.51
1-F	0.66	1993.13	8.48	7.51
1-NH_2	0.62	2082.21	6.60	5.36
1-CH_3	0.58	1994.35	6.58	4.49
2	0.88	6530.76	15.83	11.15
2-F	0.87	5857.90	15.03	11.15
2-NH_2	0.86	6032.85	14.93	11.33
2-CH_3	0.85	6436.21	14.16	11.09
3	0.85	4861.05	14.69	11.70
3a-F	0.84	4218.55	14.48	11.64
3a-NH_2	0.82	4462.95	13.38	9.65
3a-CH_3	0.81	4445.30	12.83	9.31
3b-F	0.83	4461.17	13.47	10.59
3b-NH_2	0.81	4800.12	12.59	10.32
3b-CH_3	0.80	5032.57	12.34	9.02
4	0.89	5704.97	17.29	13.64
4a-F	0.88	5007.33	17.11	13.84
4a-NH_2	0.87	5194.57	15.98	11.96
4a-CH_3	0.87	5153.96	15.96	11.87
4b-F	0.88	5190.91	16.37	13.71
4b-NH_2	0.87	5534.90	16.76	13.24
4b-CH_3	0.86	5747.23	15.79	13.01
5	0.84	4258.60	12.83	11.69
5a-F	0.83	3785.65	12.87	11.71
5a-NH_2	0.83	3830.11	12.68	10.68
5a-CH_3	0.81	3830.28	11.79	8.49
5b-F	0.82	3801.77	12.34	11.32
5b-NH_2	0.81	3715.26	12.61	10.53
5b-CH_3	0.80	3702.54	12.16	10.71
6	0.89	5894.31	19.04	14.33
6a-F	0.89	5207.60	19.02	14.34
6a-NH_2	0.88	5462.59	17.93	12.38
6a-CH_3	0.88	5417.40	17.77	12.61
6b-F	0.88	5355.28	18.03	14.30
6b-NH_2	0.88	5606.70	17.65	14.31
6b-CH_3	0.87	5882.43	17.04	13.93

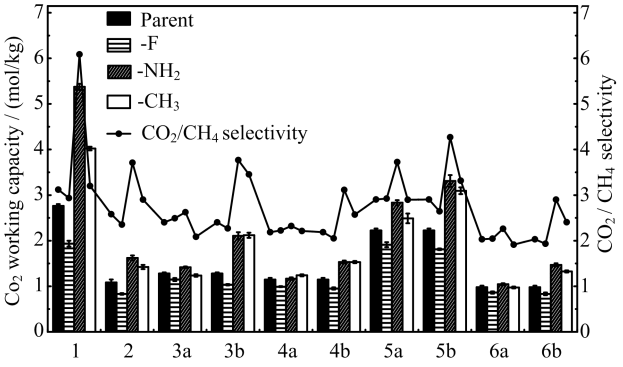

FIG. 2 CO_2 working capacity and CO_2/CH_4 selectivity of the parent and functionalized MOFs at 298 K from GCMC simulations. CO_2 working capacity was calculated as the difference in pure CO_2 uptake at 1 bar and 0.1 bar. CO_2/CH_4 selectivity was calculated from a CO_2/CH_4 mixture with the molar ratio of 1:1 at 1 bar.

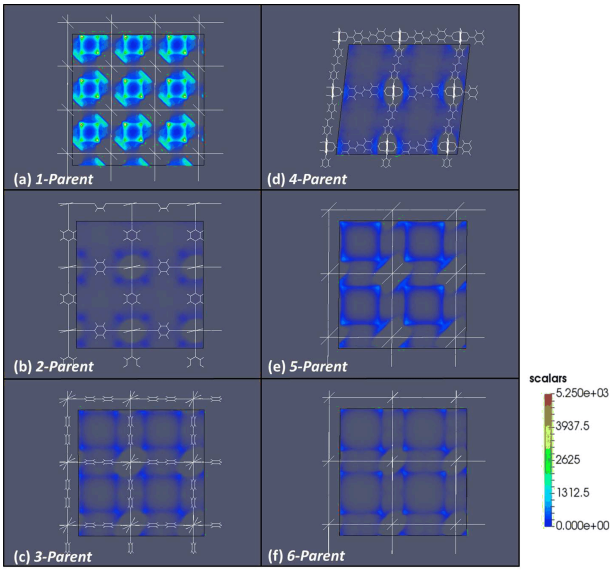

FIG. 3 Density distribution map of CO_2 adsorbates within the parent MOFs (a) 1, (b) 2, (c) 3, (d) 4, (e) 5, and (f) 6 at 298 K, 1 bar. The white lines represent the supercells of MOF frameworks and the colored regions represent the scaled adsorbate densities. All the number densities of CO_2 adsorbates were scaled by the maximum density in MOF 1 for better comparison of the adsorption capacity of the MOFs.

increased ratio of CO_2/CH_4 uptake of 3a-F and 4a-F is possibly due to a larger decrease in CH_4 uptake than CO_2 uptake compared to their parent MOFs as shown in FIG. S1 in supplementary materials, in which there is a 13.09% reduction in CH_4 uptake and 9.85% reduction in CO_2 uptake of 3a-F in contrast to MOF-3, and a 12.42% reduction in CH_4 uptake and 9.95% reduction in CO_2 uptake of 4a-F in contrast to MOF-4. On the contrary, -F functionalization of other MOFs except MOF-3 and MOF-4 resulted in a larger decrease (∼4%) in CO_2 uptake than CH_4 uptake, thus causing a reduced selectivity. However, introducing polar functionalities (such as $-NH_2$) imposes significant positive effects on the adsorption of quadrupolar CO_2 molecules compared to nonpolar CH_4 molecules, thus leading to greatly enhanced CO_2/CH_4 selectivity. It should be noted that the CO_2/CH_4 selectivity from GCMC simulation is comparable with the results of experimental

DOI:10.1063/1674-0068/31/cjcp1705108

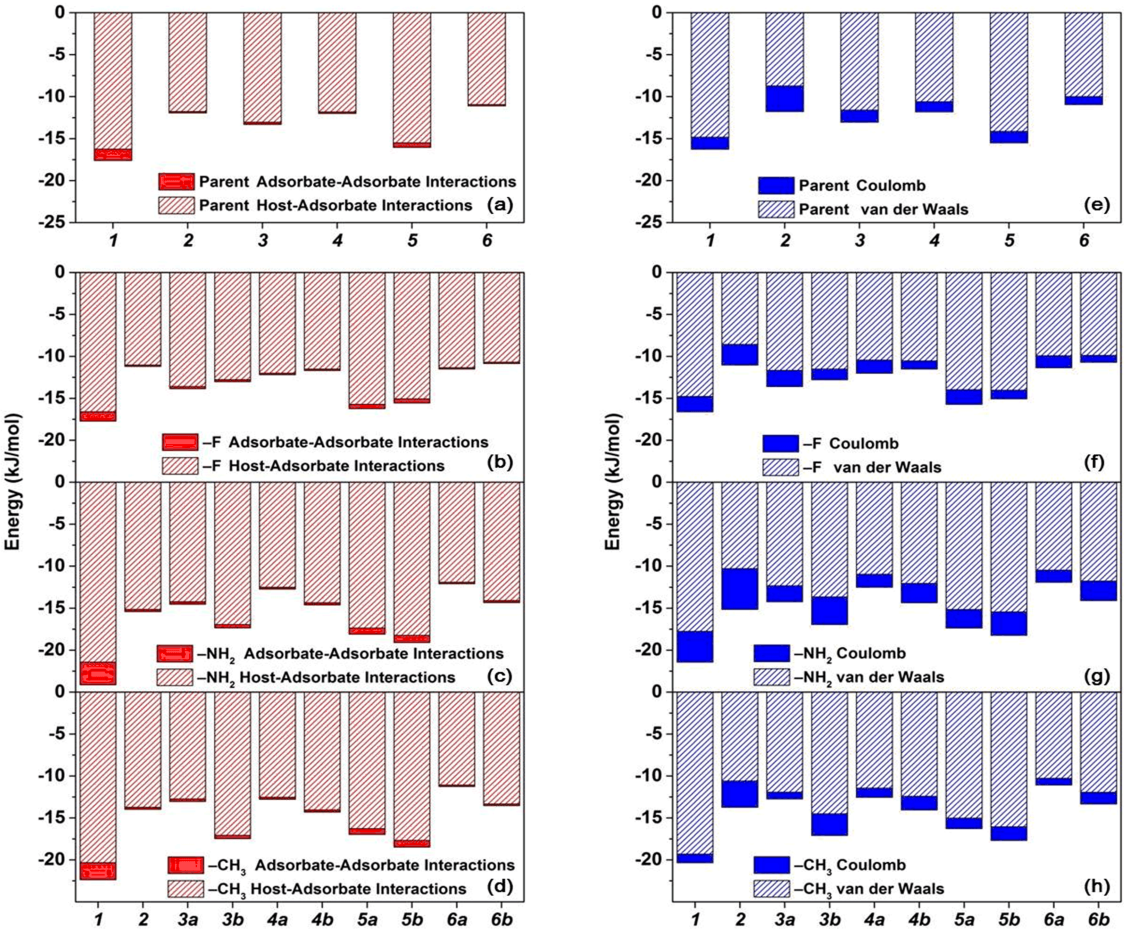

FIG. 4 The interaction energy including host-adsorbate and adsorbate-adsorbate interaction energies for (a) parent, (b) -F, (c) -NH_2, and (d) -CH_3 functionalized MOFs, as well as Coulomb and van der Waals contributions of host-adsorbate interaction energy for (e) parent, (f) -F, (g) -NH_2, and (h) -CH_3 functionalized MOFs at 1 bar.

works. Venna *et al.* [37] reported that ZIF-8 membranes exhibited a CO_2/CH_4 selectivity ranging from 4.1 to 7.0 at 99.5 kPa. Zhang *et al.* [38] also experimentally investigated a series of metal-organic materials (MOMs) whose CO_2/CH_4 selectivity ranged from 7 to 11 at 1 bar. Yang *et al.* [39] studied the CO_2/CH_4 separation performance of UiO-66(Zr) by both experimental measurements and molecular simulations, and the good agreement in CO_2/CH_4 selectivity (5−7) between experimental and computational studies was observed. With regard to modification sites, functionalization of MOFs at site b by -NH_2 and -CH_3 showed higher CO_2 working capacity than those at site a, which is probably related to the increased surface area upon functionalization. Moreover, -F functionalized MOFs at site b exhibited larger decrease in adsorption capacity and CO_2/CH_4 selectivity than those at site a. Such tendency is well supported by the total interaction energy including host-adsorbate and adsorbate-adsorbate interaction energies shown in FIG. 4.

To better comprehend the observations in FIG. 2, the computed host-adsorbate and adsorbate-adsorbate interaction energy as well as Coulombic and van der Waals contributions are shown in FIG. 4. The total interaction energy including host-adsorbate and adsorbate-adsorbate interactions within parent MOFs in FIG. 4(a) is in the order of MOF 1>5>3>4>2>6, consistent with the CO_2 adsorption working capacity shown in FIG. 2. The high interaction energy for MOF-1 can be attributed to the overlapped potential well in small pores [40]. Upon functionalization, the trend in total interaction energy is generally identical, and in general -NH_2 functionalized MOFs (FIG. 4(d)) exhibit the strongest total interaction energy followed by -CH_3 (FIG. 4(c)) and -F functionalized ones (FIG. 4(b)). Coulombic interactions between frameworks and CO_2 molecules contributed most to the host-adsorbate interaction compared to their parent or -CH_3 and -F functionalized counterparts, suggesting the strong affinity between Lewis basic -NH_2 and Lewis acid CO_2 as reported in previous work [41]. Apart from -NH_2 functionalized MOFs, -CH_3 functionalized MOFs that exhibit good adsorption performance can be traced to the strong van der Waals interactions between the guest

DOI:10.1063/1674-0068/31/cjcp1705108

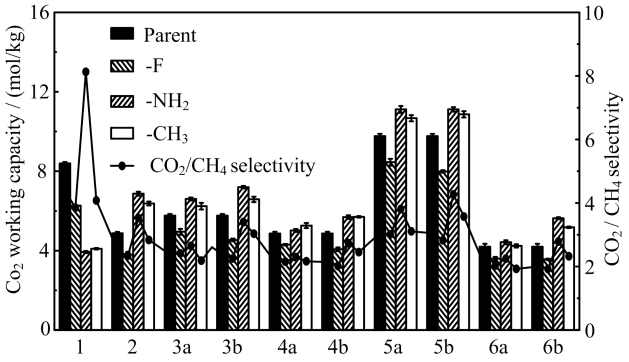

FIG. 5 CO_2 working capacity and the CO_2/CH_4 selectivity of the parent and modified MOFs at 298 K by GCMC simulations. Working capacity was calculated with pure CO_2 uptake at 5 bar subtracting that at 1 bar, while CO_2/CH_4 selectivity was calculated using a mixture of CO_2 and CH_4 with the molar ratio of 1:1.

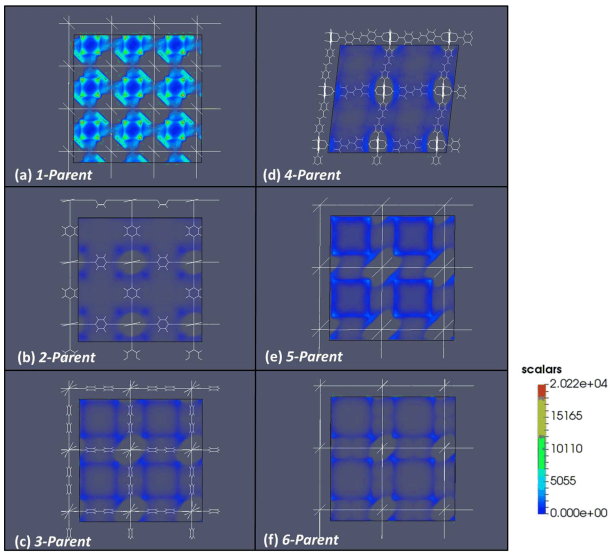

FIG. 6 Density distribution map of CO_2 adsorbates within (a) the parent MOF 1, (b) 2, (c) 3, (d) 4, (e) 5 and (f) 6 at 298 K, 5 bar. The white lines represent the supercells of MOF frameworks and the colored regions represent the adsorbates. All the number densities of CO_2 adsorbates were scaled by the maximum density in MOF 1 for better comparison of the adsorption capacity of the MOFs.

molecules and the functional groups, consistent well with the work of Walton *et al.* [20]. On the contrary, -F modified MOFs show a decreased CO_2 adsorption in contrast to their parent counterparts due to the electronic charge withdrawing nature of fluorine functional group as evidenced by DFT calculations of Torrisi *et al.* [42]. Moreover, both $-NH_2$ and $-CH_3$ functionalization at site b show a significant increase in host-adsorbate interactions compared with the functionalization at site a, hence resulting in the higher CO_2 uptake capacity and selectivity. This is probably because placing functionality at site a reduces the number of favorable adsorption sites near the metal node, leading to the slight increase in CO_2 uptake, while functionalization at site b provides additional adsorption sites within frameworks towards CO_2, thus significantly enhancing CO_2 uptake.

On the other hand, the CO_2 working capacity and CO_2/CH_4 selectivity at 5 bar of PSA conditions are shown in FIG. 5. Comparing FIG. 2 with FIG. 5, both the CO_2 working capacity and CO_2/CH_4 selectivity at 5 bar were higher than those at 1 bar. The density distribution maps of adsorbed CO_2 molecules within frameworks at 5 bar were similar to those at 1 bar (FIG. 6), and the region close to the metal node was still the favorable adsorption sites. The pores of MOF 1 were filled with CO_2 molecules (FIG. 6(a)). Moreover, the overall order of CO_2 working capacity has changed from MOF 1>5>3>4≈2>6 at the low-pressure VSA condition to 5>1>3>4≈2>6 at the high-pressure PSA condition, where MOF-5 exhibited the highest working capacity at PSA instead of MOF-1 at VSA. All functionalized MOFs of 1 have the lower CO_2 working capacity than their parent counterparts. Such an observation was mainly attributed to the smallest pores of MOF-1 (LCD=9.32 Å) among all parent MOFs, where adsorption saturation occurred at 5 bar (FIG. S2 in supplementary materials). Therefore, placing functional groups within frameworks of MOF 1 leads to the decreased CO_2 working capacity due to the reduced accessible space for CO_2 adsorption at 5 bar, which is in agreement with the findings of Babarao *et al.* [43]. Nevertheless, MOFs 2−6 exhibit increased CO_2 working capacity upon functionalization by $-NH_2$ and $-CH_3$, which is similar to the tendency observed at 1 bar. Moreover, the adsorption performance of the functionalized MOFs also falls in the order of $-NH_2$> $-CH_3$>parent>-F, similar to the observations at 1 bar of FIG. 2. The similarity in CO_2/CH_4 selectivity of 5 and 1 bar can be attributed to the almost identical impact that the pressure change imposes on CH_4 uptake and CO_2 uptake (FIG. S3 in supplementary materials). Additionally, similar to the results at 1 bar, functionalization at site b by $-NH_2$ and $-CH_3$ exhibits slightly higher CO_2 working capacity than that at site a, and -F functionalized MOFs displays the opposite tendency. However, the difference in adsorption performance of MOFs functionalized at site a and b at 5 bar is less significant than that at 1 bar.

The host-adsorbate and adsorbate-adsorbate interactions of CO_2-MOFs at 5 bar, and Coulombic and van der Waals contributions to host-adsorbate interactions are shown in FIG. 7 to help understand CO_2/CH_4 separation performance in FIG. 5. The tendency in total interaction energy of parent MOFs in FIG. 7(a) is similar to that in FIG. 4(a), consistent with their CO_2 working capacity at 1 and 5 bar except for MOF 1 due to the adsorption saturation at 5 bar. As for effects of functional groups, similar to the findings at 1 bar, the strongest Coulombic interaction was observed between $-NH_2$ functionalized MOFs and CO_2 molecules as

DOI:10.1063/1674-0068/31/cjcp1705108

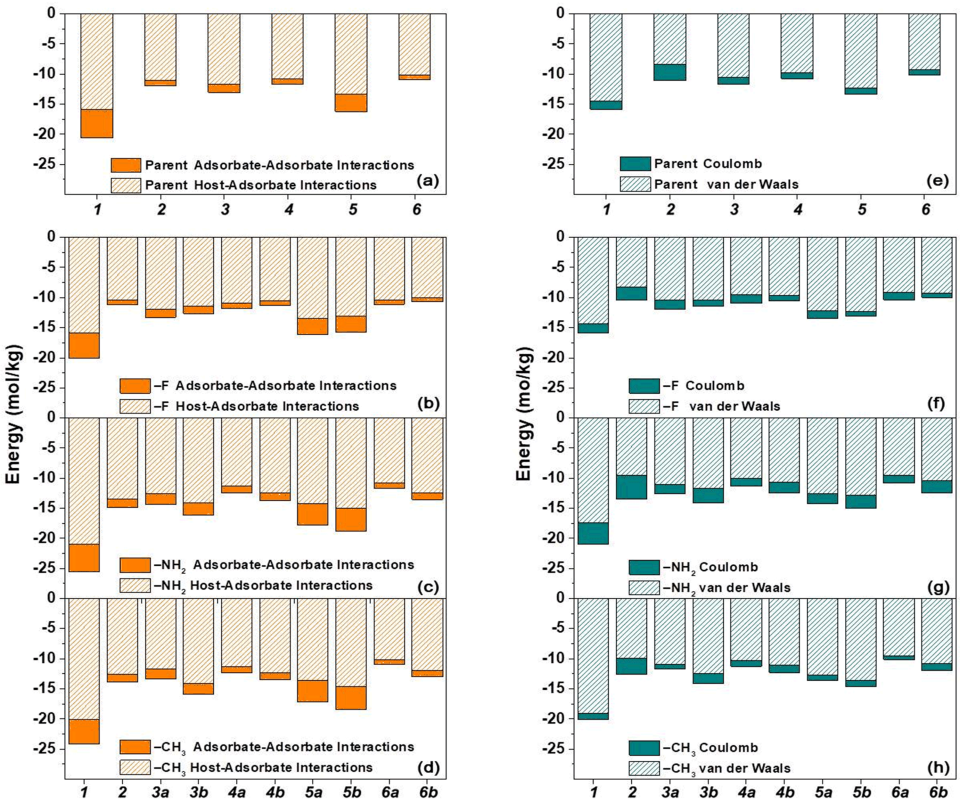

FIG. 7 Host-adsorbate and adsorbate-adsorbate interactions for (a) parent, (b) -F, (c) -NH_2 and (d) -CH_3 functionalized MOFs, as well as Coulomb and van der Waals contributions to the host-adsorbate interaction for (e) parent, (f) -F, (g) -NH_2, and (h) -CH_3 functionalized MOFs at 5 bar.

shown in FIG. 7(c), leading to the highest CO_2 working capacity at 5 bar, which is followed by -CH_3 and -F functionalized MOFs. Moreover, the host-adsorbate interactions for MOFs functionalized by -NH_2 and -CH_3 at site b are still slightly higher than those modified at site a, which also agrees with their CO_2 uptake at 5 bar. On the contrary, the host-adsorbate interaction energy of -F functionalized MOFs at site b is lower than those at site a, similar to the tendency in CO_2 working capacity.

The host-adsorbate and adsorbate-adsorbate interactions of CO_2-MOFs at 5 bar, and Coulombic and van der Waals contributions to host-adsorbate interactions are shown in FIG. 7 to help understand CO_2/CH_4 separation performance in FIG. 5. The tendency in total interaction energy of parent MOFs in FIG. 7(a) is similar to that in FIG. 4(a), consistent with their CO_2 working capacity at 1 and 5 bar except for MOF 1 due to the adsorption saturation at 5 bar. As for effects of functional groups, similar to the findings at 1 bar, the strongest Coulombic interaction was observed between -NH_2 functionalized MOFs and CO_2 molecules as shown in FIG. 7(c), leading to the highest CO_2 working capacity at 5 bar, which is followed by -CH_3 and -F functionalized MOFs. Moreover, the host-adsorbate interactions for MOFs functionalized by -NH_2 and -CH_3 at site b are still slightly higher than those modified at site a, which also agrees with their CO_2 uptake at 5 bar. On the contrary, the host-adsorbate interaction energy of -F functionalized MOFs at site b is lower than those at site a, similar to the tendency in CO_2 working capacity.

The enhancement in pure CO_2 uptake at 1 bar (FIG. 8(a)) and 5 bar (FIG. 8(b)) as well as that of the total interaction energy at 1 bar (FIG. 8(c)) and 5 bar (FIG. 8(d)) were calculated using the following equation:

$$\text{Enhancement}/\% = \frac{X_{\text{functionalized}} - X_{\text{parent}}}{X_{\text{parent}}} \times 100\% \quad (2)$$

where X refers to the CO_2 uptake or the total interaction energy of parent or functionalized MOFs. Comparing the enhancement in CO_2 working capacity, the enhancement at 1 bar (FIG. 8(a)) is generally more significant than that at 5 bar (FIG. 8(b)). Similar tendency was observed in the enhancement in the total interaction energy of MOFs at 1 bar (FIG. 8(c)) and 5 bar (FIG. 8(d)). In general, -NH_2 functionalized MOFs exhibited the most significant enhancement in CO_2 working capacity and the interaction energy, followed by -CH_3 and -F functionalized MOFs, which is similar to the former observations at 1 bar (FIG. 2 and

DOI:10.1063/1674-0068/31/cjcp1705108

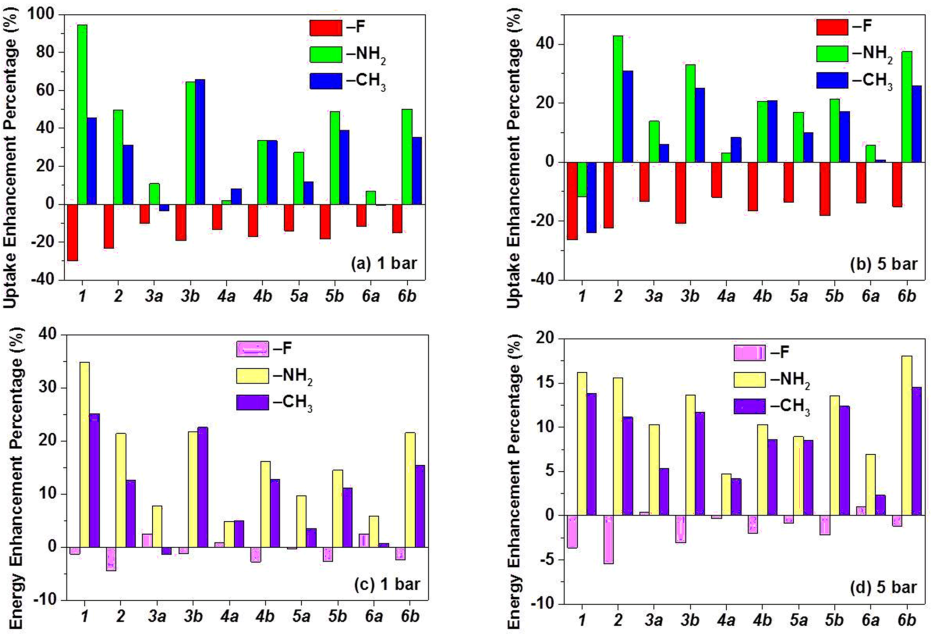

FIG. 8 Enhancement in pure CO_2 uptake of MOFs at (a) 1 bar and (b) 5 bar, and enhancement in CO_2 total interaction energy of MOFs compared with their parent counterparts at the pressure of (c) 1 bar and (d) 5 bar respectively. Computation was conducted using pure CO_2 at 298 K.

FIG. 4) and 5 bar (FIG. 5 and FIG. 7). It should be noted that the enhancement in CO_2 working capacity and interaction energy upon functionalization was only observed for -NH_2 and -CH_3 functionalized MOFs except MOF 3a-CH_3 at 1 bar and MOF 1 at 5 bar. The slightly decreased CO_2 working capacity of 3a-CH_3 at 1 bar was supported by the reduced interaction energy correspondingly in FIG. 8(c). As demonstrated previously, functionalization at site a reduced the number of favorable adsorption sites around the metal node compared with 3b-CH_3, leading to the slightly decreased adsorption of 3a-CH_3. For MOF 1-NH_2 and 1-CH_3 at 5 bar, although their total interaction energy was increased compared with their parent, the CO_2 working capacity was decreased, which can be attributed to the limited space for CO_2 adsorption. In addition, all -F functionalized MOFs exhibited decreased CO_2 working capacity in contrast to their unfunctionalized counterparts regardless of the increased or decreased interaction energy, consistent with the observations in FIG. 2 and FIG. 5.

IV. CONCLUSION

As an effective strategy of improving CO_2/CH_4 separation performance of MOFs, functionalization is frequently employed experimentally and theoretically. In this work, we employed GCMC simulations to study the impact of different functional groups at varying modification sites on their CO_2/CH_4 separation performance in MOFs with pcu topology and six types of linkers. CO_2 working capacity shows pore-size dependence, and parent MOF structures with smaller pores generally have larger CO_2 uptake. MOF-1 with the smallest pores exhibited the highest uptake upon functionalization at 1 bar, but a slight increment and even a decrement compared to parent MOFs at 5 bar. This observation sheds light on the importance of tailoring the pore size of MOFs at different operation conditions to balance between the gain in framework-adsorbate affinity due to potential well overlap in small pores and the loss of available adsorption sites. Moreover, the performance of different functional groups decrease in the order of -NH_2 >-CH_3>-F, rendering guidance in the choice of functionalities in synthetic process. Placing the functional groups at site b imposed more obvious impact on CO_2 adsorption due to the introduction of additional adsorption sites compared to that at site a. Besides, both the influence of different functional groups and modification sites are more evident at 1 bar compared to that at 5 bar, because the host-adsorbate interactions play a more dominant role in CO_2 adsorption at low pressures. Our findings have shown the interplay among pore size, functional groups, modification sites and operation conditions for applications. We believe this work will guide synthetic experiments to design MOFs with improved adsorption capacity and selectivity for CO_2/CH_4 separation. However, further efforts are needed to extrapolate such findings to MOFs of other topologies.

Supplementary materials: FIG. S1 shows CH_4 uptake of the MOFs with the molar ratio of CO_2:CH_4=1:1,

DOI:10.1063/1674-0068/31/cjcp1705108

FIG. S2 shows pure CO_2 adsorption isotherms of MOF 1 and 5, and CO_2/CH_4 selectivities of all MOF structures with a molar ratio of CO_2:CH_4=1:1 are also provided.

V. ACKNOWLEDGMENTS

This work was supported by the National Natural Science Foundation of China (No.51606081) and the Basic Research Foundation of Shenzhen (No.JCYJ20160506170043770).

[1] D. Andriani, A. Wresta, T. D. Atmaja, and A. Saepudin, Appl. Biochem. Biotechnol. **172**, 1909 (2014).
[2] Y. S. Bae and R. Q. Snurr, Angew. Chem. Int. Ed. Engl. **50**, 11586 (2011).
[3] Y. Zhang, J. Sunarso, S. M. Liu, and R. Wang, Int. J. Greenhouse Gas Control **12**, 84 (2013).
[4] R. T. Yang, *Gas Separation by Adsorption Processes*, Boston: Butterworth-Heinemann, (2013).
[5] J. L. C. Rowsell and O. M. Yaghi, J. Am. Chem. Soc. **128**, 1304 (2006).
[6] P. Huang and L. Yan, Chin. J. Chem. Phys. **29**, 742 (2016).
[7] H. G. Song, Y. J. Ding, J. Yang, and H. X. Xu, Chin. J. Chem. Phys. **29**, 693 (2016).
[8] H. C. Zhou and S. Kitagawa, Chem. Soc. Rev. **43**, 5415 (2014).
[9] X. H. Zhou, H. H. Li, and W. Huang, Chin. J. Struc. Chem. **31**, 33 (2012).
[10] S. Cavenati, C. A. Grande, A. E. Rodrigues, C. Kiener, and U. Mller, Ind. Eng. Chem. Res. **47**, 6333 (2008).
[11] J. R. Li, J. Sculley, and H. C. Zhou, Chem. Rev. **112**, 869 (2012).
[12] C. E. Wilmer, O. K. Farha, Y. S. Bae, J. T. Hupp, and R. Q. Snurr, Energy Environ. Sci. **5**, 9849 (2012).
[13] Y. S. Bae, K. L. Mulfort, H. Frost, P. Ryan, S. Punnathanam, L. J. Broadbelt, J. T. Hupp, and R. Q. Snurr, Langmuir **24**, 8592 (2008).
[14] M. Eddaoudi, J. Kim, N. Rosi, D. Vodak, J. Wachter, M. O'keeffe, and O. M. Yaghi, Science **295**, 469 (2002).
[15] H. X. Deng, C. J. Doonan, H. Furukawa, R. B. Ferreira, J. Towne, C. B. Knobler, B. Wang, and O. M. Yaghi, Science **327**, 846 (2010).
[16] J. G. McDaniel, K. Yu, and J. R. Schmidt, J. Phys. Chem. C **117**, 17131 (2013).
[17] M. G. Frysali, E. Klontzas, E. Tylianakis, and G. E. Froudakis, Microporous Mesoporous Mater. **227**, 144 (2016).
[18] R. Banerjee, H. Furukawa, D. Britt, C. Knobler, M. O'Keeffe, and O. M. Yaghi, J. Am. Chem. Soc. **131**, 3875 (2009).
[19] Q. Y. Yang, A. D. Wiersum, P. L. Llewellyn, V. Guillerm, C. Serre, and G. Maurin, Chem. Commun. **47**, 9603 (2011).
[20] H. Jasuja, J. Zang, D. S. Sholl, and K. S. Walton, J. Phys. Chem. C **116**, 23526 (2012).
[21] S. Couck, J. F. M. Denayer, G. V. Baron, T. Rémy, J. Gascon, and F. Kapteijn, J. Am. Chem. Soc. **131**, 6326 (2009).
[22] W. Mu, D. H. Liu, Q. Y. Yang, and C. L. Zhong, Microporous Mesoporous Mater. **130**, 76 (2010).
[23] D. A. Gomez-Gualdron, O. V. Gutov, V. Krungleviciute, B. Borah, J. E. Mondloch, J. T. Hupp, T. Yildirim, O. K. Farha, and R. Q. Snurr, Chem. Mater. **26**, 5632 (2014).
[24] J. J. Potoff and J. I. Siepmann, AIChE J. **47**, 1676 (2001).
[25] A. K. Rappé, C. J. Casewit, K. S. Colwell, W. A. Goddard III, and W. M. Skiff, J. Am. Chem. Soc. **114**, 10024 (1992).
[26] G. A. Kaminski, R. A. Friesner, J. Tirado-Rives, and W. L. Jorgensen, J. Phys. Chem. B **105**, 6474 (2001).
[27] P. G. Boyd, S. M. Moosavi, M. Witman, and B. Smit, J. Phys. Chem. Lett. **8**, 357 (2017).
[28] J. G. McDaniel, S. Li, E. Tylianakis, R. Q. Snurr, and J. R. Schmidt, J. Phys. Chem. C **119**, 3143 (2015).
[29] G. Kresse and J. Furthmüller, Phys. Rev. B **54**, 11169 (1996).
[30] G. Kresse and J. Hafner, Phys. Rev. B **47**, 558 (1993).
[31] G. Kresse and J. Hafner, Phys. Rev. B **49**, 14251 (1994).
[32] D. Dubbeldam, S. Calero, D. E. Ellis, and R. Q. Snurr, Mol. Simul. **42**, 81 (2016).
[33] U. Essmann, L. Perera, M. L. Berkowitz, T. Darden, H. Lee, and L. G. Pedersen, J. Chem. Phys. **103**, 8577 (1995).
[34] S. Cavenati, C. A. Grande, and A. E. Rodrigues, J. Chem. Eng. Data **49**, 1095 (2004).
[35] T. F. Willems, C. H. Rycroft, M. Kazi, J. C. Meza, and M. Haranczyk, Microporous Mesoporous Mater. **149**, 134 (2012).
[36] Q. Y. Yang, C. L. Zhong, and J. F. Chen, J. Phys. Chem. C **112**, 1562 (2008).
[37] S. R. Venna and M. A. Carreon, J. Am. Chem. Soc. **132**, 76 (2010).
[38] Z. J. Zhang, W. Y. Gao, L. Wojtas, S. Q. Ma, M. Eddaoudi, and M. J. Zaworotko, Angew. Chem. Int. Ed. Engl. **51**, 9330 (2012).
[39] Q. Y. Yang, A. D. Wiersum, H. Jobic, V. Guillerm, C. Serre, P. L. Llewellyn, and G. Maurin, J. Phys. Chem. C **115**, 13768 (2011).
[40] N. C. Burtch, H. Jasuja, D. Dubbeldam, and K. S. Walton, J. Am. Chem. Soc. **135**, 7172 (2013).
[41] S. Choi, T. Watanabe, T. H. Bae, D. S. Sholl, and C. W. Jones, J. Phys. Chem. Lett. **3**, 1136 (2012).
[42] A. Torrisi, C. Mellot-Draznieks, and R. G. Bell, J. Chem. Phys. **130**, 194703 (2009).
[43] R. Babarao, C. J. Coghlan, D. Rankine, W. M. Bloch, G. K. Gransbury, H. Sato, S. Kitagawa, C. J. Sumby, M. R. Hill, and C. J. Doonan, Chem. Commun. **50**, 3238 (2014).

DOI:10.1063/1674-0068/31/cjcp1705108